中国激光

仿生竹纤维五系铝基复合结构强-韧性调控与界面显微组织研究(特邀)

杨光[1*]，马一鑫[1]，赵朔[2**]，钦兰云[1]，王向明[3]

[1]沈阳航空航天大学机电工程学院，辽宁 沈阳 110136；

[2]沈阳航空航天大学航空制造工艺数字化国防重点学科实验室，辽宁 沈阳 110136；

[3]航空工业沈阳飞机设计研究所，辽宁 沈阳 110035

摘要 为进一步提高铝基复合材料的强度与韧性，避免强韧性倒置关系，通过在铝基体中加入不同体积分数与尺寸的钛合金骨架结构，制备出强韧性可调控的仿竹纤维 Al-Ti 复合结构。研究发现：钛合金强化骨架与铝合金基体界面间发生了扩散反应，形成了致密的冶金结合，界面内析出相为钛铝金属间化合物。与传统铝基复材相比，复合结构铝基复合材料抗压强度高达 380～1085 MPa，形成一体化微/宏观“高强-高韧”纤维状复合结构。对微观变形机制进行研究：高强度化合物的析出有效阻止了异质界面内裂纹萌生、扩展。同时高分辨下观察发现，界面内析出的 Ti_3Al 相变形后在晶粒内部形成了有效的变形孪晶，提升了界面内高、低模量析出相间协调变形能力，是复合结构增强-增韧的主要机制。

关键词 激光技术；增材制造；仿生结构；Al-Ti 复合结构材料；微/宏观强韧性调控

中图分类号 TN249 **文献标志码** A **DOI**：10.3788/CJL231501

1 引 言

铝基复合材料(AMCs)不仅继承了传统铝合金的特点，在实现轻量化的同时，其综合性能显著提高[1-2]。目前，为了满足减重、减振、高寿命等应用需求，AMCs 被应用在诸多领域：航空航天领域飞行器腹鳍、直升机旋翼系统连接部件、航空发动机风扇叶片、卫星天线支架、平台等；交通方面汽车发动机活塞抗磨环、汽车连杆等零部件以及电子领域的功能件等[3-5]。然而，利用传统方法制备 AMCs，成本高的同时工艺复杂，成形材料易出现强度和断裂韧性互斥现象。如何获得高强高韧结构 AMCs 成为了亟需解决的难题，除了考虑增强体和基体的材料选择外，制备方法和空间结构的设计对于构建 AMCs 也起着至关重要的作用。通过传统的制备技术，如铸造和粉末冶金等，很难同时实现对增强相的微/宏观调控[6]。增材制造(AM)突破传统制造方法，利用层层叠加的原理[7-8]，实现多自由度制造高精度和复杂的点阵结构[9-10]，在精确调节相演变以及组分和结构的分布方面，定制结构和合成多种材料中的自由形式使得该工艺更适合发展异质结构。

目前已有研究学者提出了根据自然界中现存的生物结构，通过调控微结构来设计复合材料的力学性能，以期协同优化材料的强度和韧性[11]。Sun 等[12]提出了一种仿虾蛄结构的具有高损伤容限的陶瓷复合材料，其韧性比传统陶瓷结构提高了约 116 倍。Liu 等[13]采用激光选区熔融制备技术设计并制备了体积分数为 14% 的 TC4 支撑结构，再填充纯钛粉后经热等静压工艺，得到了珍珠状结构复合材料，其抗弯强度约为 1150 MPa，高于纯钛的 800 MPa，裂纹萌生强度可达 48.7 $MPa\cdot m^{1/2}$，高于纯钛的 26.1 $MPa\cdot m^{1/2}$。Zhang 等[14]通过制备铜合金仿生鱼鳞组织，将铜熔体渗透到不同的龙虾钳(bouligand)式结的钨纤维中，获得了强度和延展性协同增强的 Cu-W 合金，与传统烧结的 Cu-W 合金相比，双 bouligand 结构的抗拉极限提高了 4.1 倍，延伸率可达(20±3)%。Zhang 等[15]通过将纯镁熔融体渗透到电子选区熔融制备的 TC4 骨架中，制备了鲍鱼壳(砖混)、bouligand 和珍珠壳(交叉层状)三种仿生类型的 Mg-Ti 复合结构，复合材料的强度明显高于纯 Mg，但延展性低于纯 Mg。值得一提的是，交叉层状结构在性能上发挥协同增强作用，使断裂韧性提高约 2.7 倍。由此看来，仿生学结构为实现高性能材料提供了一种新的思路。五系铝合金具有轻质、良好的可焊性、优异的比强度和高延展性等特点，因此被用作商用和军用飞机的主要结构材料，这对铝合金的高断

收稿日期：2023-12-11；**修回日期**：2024-01-29；**录用日期**：2024-01-30；**网络首发日期**：2024-02-20

基金项目：国家重点研发计划(2022YFB4600901)、国家自然科学基金(52375359)、辽宁省国际科技合作计划(2023JH2/10700024)

通信作者：*yangguang@sau.edu.cn；**szhaosau@163.com

裂韧性提出了更高的要求，用以满足损伤容限设计标准。然而，韧性和强度往往互斥，限制了铝合金的应用。本文参考竹纤维轴向强度优异于截面方向[16]，且层状轴状竹纤维高强韧性的特点[17]，提出沿一维方向改善其强度与韧性，具体方法是：在真空条件下将铝合金熔渗到AM的TC4骨架结构中，形成金属-金属贯穿连续复相强化结构，实现轻量化的同时大幅提升铝基复合结构材料。

2 试验及方法

2.1 钛合金强化骨架增材制备及铝合金基体熔炼工艺

为了实现强化相与铝合金基体致密的冶金结合，如图1所示，本研究采用两步实验法：首先，采用激光粉末床熔融沉积（LPBF）技术制备仿竹纤维的TC4骨架结构，其单元直径分别为3 mm、4 mm、5.2 mm、6 mm，高为14 mm，分别占总体积的18.4%、32.2%、58.5%、72.6%。具体工艺流程为：以粒度为15～53 μm的TC4粉末作为原料（化学成分见表1），采用BLT-S210设备在高纯度的氩气中成形，激光束光斑直径为0.1 mm，激光扫描方式为三维动态振镜聚焦，具体工艺参数见表2，在扫描过程中，扫描角度在连续层间逆时针旋转67°交替进行。骨架制备完毕，用铝合金碎块对TC4骨架进行填充熔炼处理，铝合金的化学成分见表1，真空熔炼工艺参数见表3。

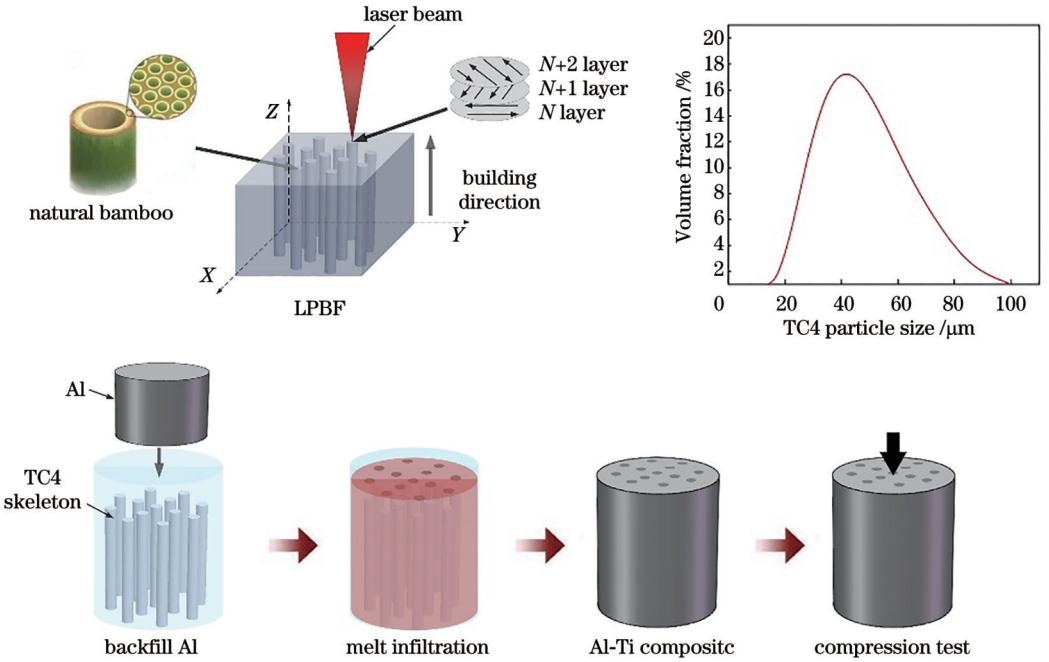

图1 Al-Ti复合材料制备工艺

Fig. 1 Preparation process of Al-Ti composites

表1 TC4与Al-Mg-Sc-Zr的化学成分

Table 1 Chemical compositions of the TC4 and Al-Mg-Sc-Zr

Material	Mass fraction /%							
	Ti	Al	Mg	V	Fe	Sc	Mn	Zr
TC4	Bal.	5.5–6.8	—	3.5–4.5	≤0.30	—	—	—
Al-Mg-Sc-Zr	0.15	Bal.	4.0–5.0	—	≤0.40	0.6–0.8	0.3–0.8	0.2–0.5

表2 LPBF工艺的参数

Table 2 Parameters of LPBF process

Parameter	Laser power /W	Scanning speed /(mm·s^{-1})	Layer thickness /mm	Hatch spacing /mm
Value	155	1200	0.03	0.09

表3 真空熔炼工艺的参数

Table 3 Parameters of vacuum melting process

Parameter	Heating rate /(℃/min)	Heating temperature /℃	Holding time /min	Cooling method
Value	8	800	60	Furnace cooling

2.2 显微组织表征

利用JEOL7900F扫描电子显微镜(SEM)对复合材料横截面的显微组织进行观察,电子加速电压为15 kV,工作距离为10.5 mm。利用SEM配备的定量X射线能谱仪(EDS)分析相的化学组成和元素分布情况。同时,为了明确变形机理,利用Thermo Scientific Scios-2型FIB-SEM系统在靠近裂纹处制备了透射电子显微镜(TEM)观察实验样品,通过Thermofisher Talos F200X透射电子显微镜在200 kV加速电压下对样品的微观结构进行了研究分析。

2.3 力学性能研究

利用Bruker纳米压痕仪对试样的不同区域进行试验,在连续刚度测量模式下,选择Berkovich尖端(半径为273 nm)的三面金刚石尖端进行压痕,在加载速率为40 μN/s的条件下,最大载荷为6000 μN,保载2 s。室温压缩试验采用Instron 5982电子万能试验机,加载速度为0.5 mm/min,为了避免尺寸效应,压缩试样均为尺寸相同的圆柱体,直径为7 mm,高为14 mm,长径比为2.0,如图2所示。

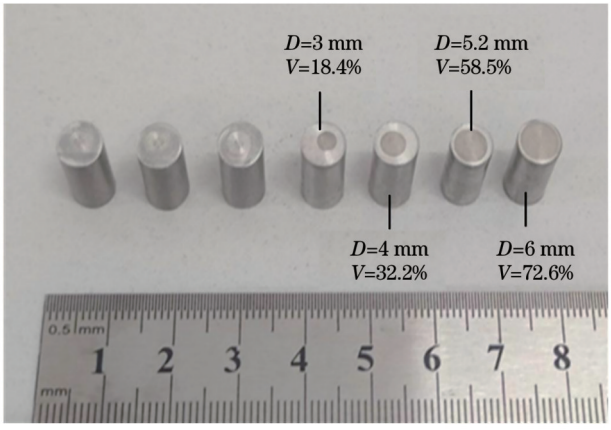

图2 压缩试样

Fig. 2 Compression specimen

3 分析与讨论

3.1 钛合金增强铝基复合结构微/宏观界面组织

为了研究钛合金骨架与铝合金基体间的结合情况,对复合结构的截面组织形貌进行显微分析,结果如图3(a)所示,复合结构中较亮的白色圆形区域为TC4骨架,较暗的灰色区域为铝合金,TC4骨架与铝合金之间存在明显的粗糙界面反应层,厚度约为600 μm。图3(c)为TC4区域的SEM图像,可见,大部分为灰色针状α相,少量白色β相沿着α相相界处分布,形成交织的网篮组织。图3(d)~(f)为界面反应层内由TC4骨架过渡到铝基体的组织形貌,可以观察到靠近TC4骨架的析出相大多为尺寸较小的等轴晶,少量柱状晶,且随着距离的增加,析出相逐渐变大,为粗大的板条状,结合微区成分分析,可以确定各析出相的原子比。将EDS结果与微区形貌[表4,图3(d)]对比,发现反应层内存在Ti、Al原子比近似为1∶1、1∶3、3∶5以及1∶2的析出相。结合前期相关研究结果[18-19],对生成的界面附近元素分布情况进行表征,从图3(g)可以看出,Al元素以及少量Ti和V元素扩散到连续界面中,而Ti元素在熔渗过程中几乎没有扩散到熔融铝合金中,整个反应过程为固液结合,这在之前的研究中已得到了证实[20-21]。此外,观察到铝合金中的Zr元素和Sc元素明显富集在界面反应层最外层,这与Sc、Zr元素与Ti、Al元素的结合能力的差异有关。图3(h)显示Ti和Al沿着界面呈相反的浓度梯度分布,且Ti/Al的分布比在两相金属界面中显著波动,说明界面反应层生成了多种金属间化合物,这些复杂的金属间化合物在应力下的变形方式与显微结构直接影响异质界面结合的结合性与变形性。同时,根据早期的研究发现[22],对于钛合金和铝合金间扩散反应生成的界面,温度和保温时间是控制析出相的最关键的问题,少量的金属间化合物可以提高界面的结合质量,过厚的界面,反而恶化复合材料的力学性能,因此优化熔炼工艺,调整界面微观结构是异质合金成形的关键。

3.2 铝基复合结构协调变形能力研究

为了探究复合结构在压应力下的变形机制,对样品进行纳米压痕和单轴压缩试验。图4(a)为样品的纳米压痕载荷-位移曲线,从图中可以观察到各个区域的加载曲线都是光滑的,且均表现为弹性变形。界面内析出相最大压入深度为100 nm,TC4骨架最大压入深度为150 nm,而铝合金基体最大压入深度为500 nm。图4(b)统计了不同区域的显微硬度值:界面析出相硬度为6.59 GPa,TC4骨架的微区硬度为4.62 GPa,铝基体的微区硬度为0.8 GPa,图4(c)为室温下轴向施加载荷后铝基复合结构宏观真实应力-应变曲线,纯TC4合金抗压强度为1494 MPa,铝合金基体的抗压强度为270 MPa,当TC4骨架的直径尺寸为3 mm、4 mm、5.2 mm、6 mm,对应体积分数为18.4%、32.2%、58.5%、72.6%时,铝基复合结构的抗压强度分别为380 MPa、579 MPa、916 MPa、1085 MPa,且在材料屈服前弹性应变量分别为3.3%、7.6%、5.8%、7.2%。而TC4合金的弹性应变量为6.2%,铝合金基体的弹性应变量为2.1%。可以看出,随着抗压强度的升高,复合结构断裂前弹性变形量并没有大幅减小,有效避免了强韧性倒置关系。结果表明复合结构界面内析出相硬度、整体抗压强度以及韧性明显高于铝基体,且抗压强度随着TC4骨架体积分数的增加而增加,这是由于TC4骨架与基体之间的连续性,以及界面处硬质金属间化合物的析出,提高了复合结构界面的结合能力。同时,结合透射观察发现,界面析出相具有一定的变形能力,可以更好地传递应力,增强TC4骨架结构在复合结构中的强化效果,从而提高了整体强韧性。

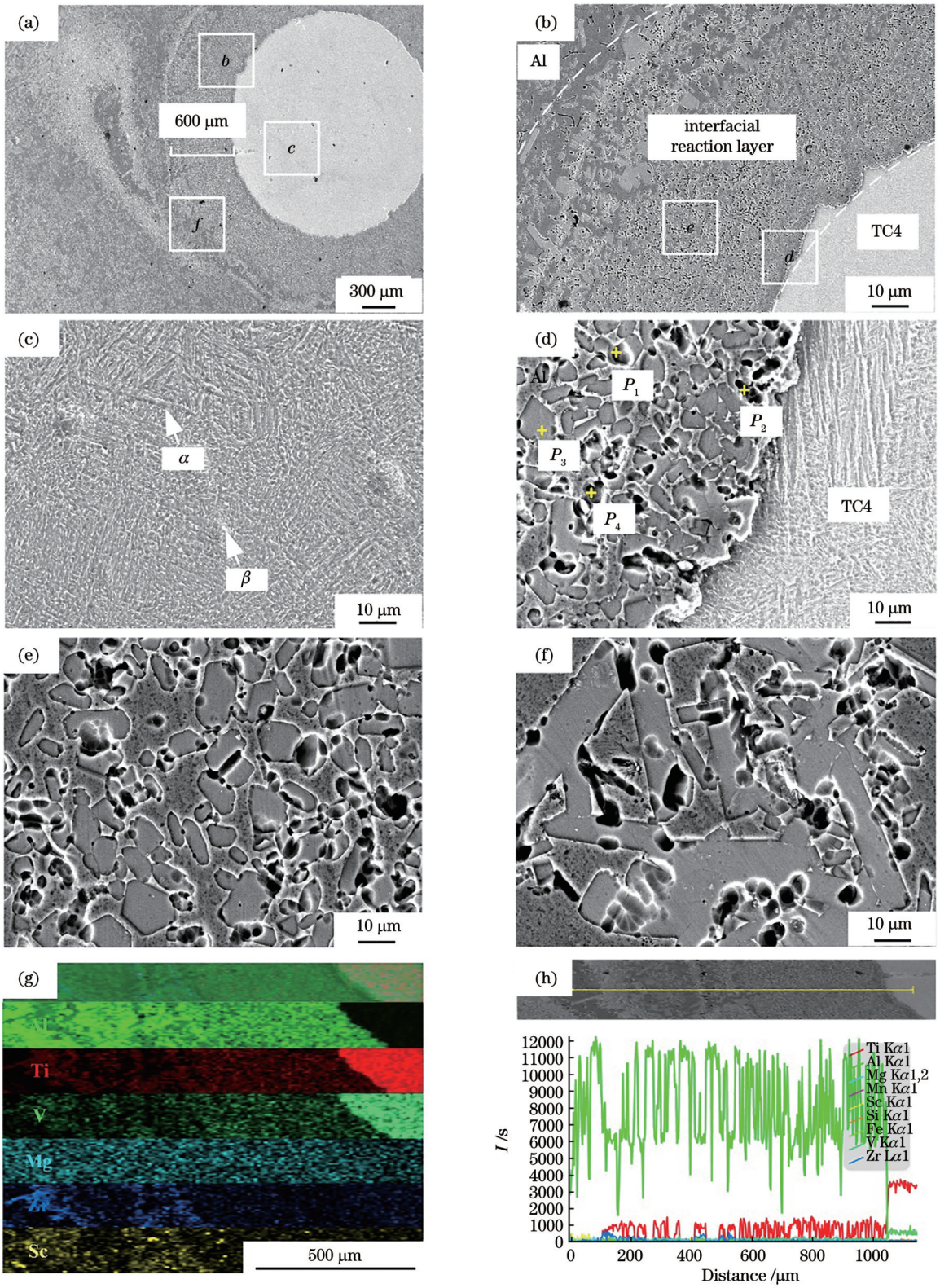

图 3 铝基复合结构的SEM图像。(a)界面内及界面附近钛/铝基体组织;(b)反应生成的界面形貌;(c)熔炼后TC4骨架显微组织;(d)界面内靠近TC4骨架的析出相形貌;(e)界面内中间区域的析出相形貌;(f)界面内靠近铝基体的析出相形貌;(g)界面附近元素分布;(h)界面及界面附近定量元素分布统计

Fig. 3 SEM images of an aluminum-based composite structure. (a) Titanium/aluminum matrix organization at and near the interface; (b) reaction-generated interface morphology; (c) TC4 skeleton microstructure after melting; (d) precipitation phase morphology in the interface near the TC4 skeleton; (e) precipitation phase morphology in the middle region of the interface; (f) precipitation phase morphology in the interface near the aluminum matrix; (g) elemental distribution near the interface; (h) distribution statistics of quantitative elements in and around the interface

表 4 界面内析出相成分分析

Table 4 Compositional analysis of precipitated phases within the interface

Element	Atomic fraction /%			
	P_1	P_2	P_3	P_4
Ti	36.9	47.8	35.5	72.3
Al	60.0	48.0	62.3	25.2

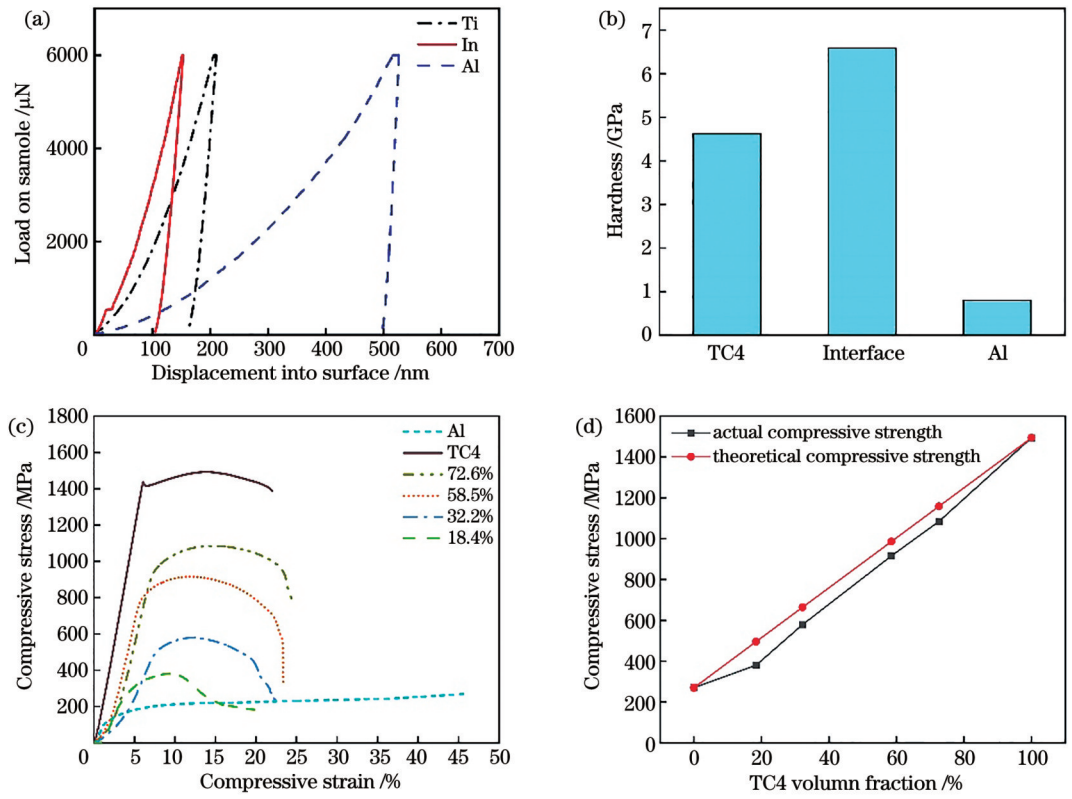

图 4 铝基复合结构的力学性能。(a)载荷-压入深度曲线;(b)不同区域硬度统计;(c)压缩应力-应变曲线;(d)实际、理论抗压强度对比

Fig. 4 Mechanical properties of aluminum-based composite structures. (a) Load-indentation depth curves; (b) hardness statistics for different regions; (c) compressive stress-strain curves; (d) comparison of actual and theoretical compressive strengths

将含有不同钛合金骨架体积分数的铝基复合结构压缩强度与传统非均质复合材料混合规则进行对比。根据强度混合定律(ROM),硬组织与软组织混合后,复合结构的抗压强度 σ_{total}[23]可表示为

$$\sigma_{total}=\sigma_{Ti}V_{Ti}+\sigma_{Al}V_{Al}, \tag{1}$$

式中:σ_{Ti}、σ_{Al}和 V_{Ti}、V_{Al}分别是复合结构两相的抗压强度和有效体积分数。压缩过程中,复合结构中的 TC4 和铝合金的抗压强度分别为 1494 MPa 和 270 MPa。由式(1)可求出不同强化体积分数下的复合结构预测抗压强度 σ_{total},如表 5 所示。图 4(d)反映了复合结构的真实抗压强度和混合定律预测值对比情况,研究发现,预测的抗压强度高于相应的实测值,这是由铝基体的应变局部化引起的[24],在压缩过程中,铝基体的流动应力高于 TC4 骨架,当铝基体发生塑性形变时,TC4 骨架仍处于弹性变形阶段,使复合材料在外加应力下容纳较大的宏观塑性应变[25-26]。图 5(c)和(d)为压缩后试样表面的显微组织,可以看出当试样在压应力下,外层的铝合金表面出现明显的塑性变形,形成具有沿 45°方向的流线型剪切带[27],这是由于在塑性变形全过程中,软/硬区因塑性不相容在界面处产生内应力[28-30],发生不均匀变形时诱发异质变形(HDI),并由软区背应力引发额外的 HDI 强化,直到背应力非常高的点可以穿透边界,在界面处形成微裂纹,微裂纹倾向在剪切带中萌发并沿着剪切带的方向迅速扩展,使复合材料沿着最大切应力方向(θ_T=45°)发生断裂。HDI 强化机制可以提高整体屈服强度,并在两个区域的塑性变形过程中诱发额外的 HDI 硬化。复合材料的实际抗压强度与 TC4 的体积分数呈线性关系,对 TC4 的体积分数为 18.4%、32.2%、58.5%、72.6% 的四组数据进行线性拟合,公式为

$$y=12.96x+151.5,\ 18\leqslant x\leqslant 100, \tag{2}$$

式中:x 为 TC4 骨架的体积分数;y 为复合结构的抗压强度。

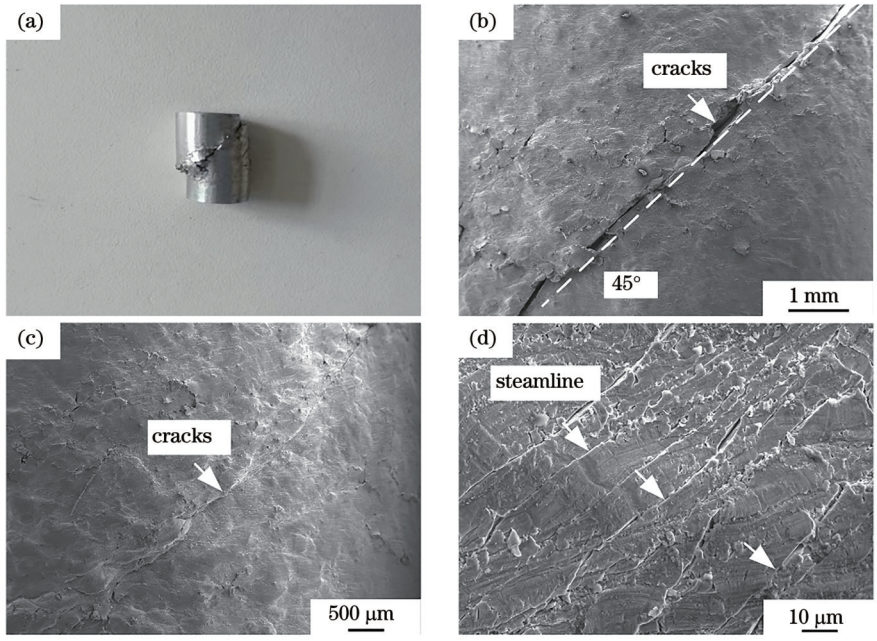

图 5 压溃样品的表面形貌。(a)宏观形貌;(b)裂纹宏观形貌;(c)裂纹微观形貌;(d)裂纹附近变形带

Fig. 5 Surface morphology of crushed sample. (a) Macroscopic morphology; (b) macroscopic morphology of the crack; (c) microscopic morphology of the crack; (d) streamline near the crack

表 5 铝基复合结构理论抗压强度与实际抗压强度

Table 5 Theoretical and actual compressive strength of composite structures

TC4 volume fraction /%	Pillar diameter /mm	Actual compressive strength /MPa	Theoretical compressive strength /MPa	Predicted compressive strength /MPa	Absolute error /%
100.0	0	1494	1494.00	1447.50	3.1
0	0	270	270.00	151.50	—
18.4	3.0	380	495.22	389.96	2.6
32.2	4.0	579	664.13	568.81	1.8
58.5	5.2	916	986.04	909.66	0.7
72.6	6.0	1085	1158.62	1092.40	0.7

3.3 钛合金骨架强化铝基复合结构界面强韧化机理

界面内软相与硬相之间的协调变形能力是决定复合材料力学特性的关键,为了进一步观察界面内金属间化合物在应力下的变形机制,利用高分辨透射电镜(HRTEM)观察、揭示压缩变形后界面的内组织结构与位错情况。图 6(a)为高角度环形暗场扫描透射电子显微镜(HAADFSTEM)图像,图中各元素分布情况分别如图 6(b)~(h)所示,可以看出 Ti、V、Sc、Zr 等元素主要分布在析出相内区域,Al、Mg 元素主要分布在基体区域。同时,在暗场下观察发现[图 7(a)]界面内析出相周围存在着大量的几何必要位错,说明这种高强度的析出相在软的基体内具有一定的协调变形能力,这种软和硬相之间界面附近的位错堆积可以补偿两相直接的应力不匹配[30]。与均匀材料相比,位错的堆积对应于背应力硬化效应,提高了复合材料的应变硬化能力。图 7(c)析出相的暗场图像中可以看出析出的硬质相内部出现了明显的位错和变形孪晶结构,根据相关的 SAED 模式推断,析出相为 Ti_3Al,该相具有明显的变形强化形式和大量的变形吸收能量的能力,孪晶的引入将进一步阻碍位错形成与传递[31-33],阻止裂纹扩展,使复合材料表现出优异的韧性。

4 结 论

利用激光选区熔化技术和真空熔炼技术制备了一种强韧性可调控 Al-Ti 金属基复合结构,对微观组织特征、压缩性能、界面内析出相晶体结构进行分析,探究增强体体积分数与强-韧性之间关系,得出以下结论。

1) 通过调节真空熔炼温度,可以获得界面致密结合的铝/钛复合结构,反应生成界面厚度约为 600 μm,界面内析出相为硬度较高的钛铝金属间化合物。

2) 铝/钛复合结构具有良好的强度和韧性,通过调节钛合金骨架体积分数,调整复合结构宏观强/韧性,抗压强度变化范围为 380~1085 MPa,是铝基体

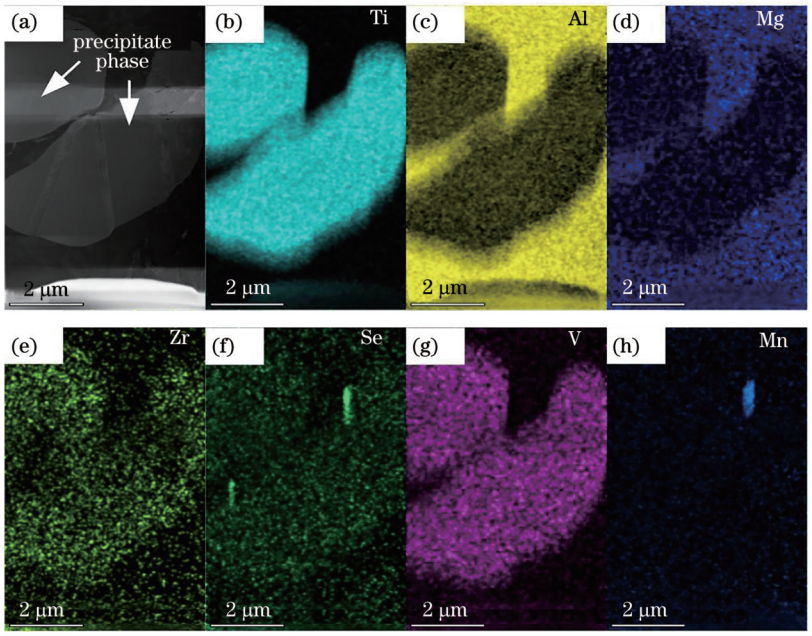

图 6　界面的 TEM 图像。(a)HAADF-STEM 图;(b)~(h)EDS 映射图像

Fig. 6　TEM images of the interface. (a) HAADF-STEM images; (b)–(h) EDS mapping images

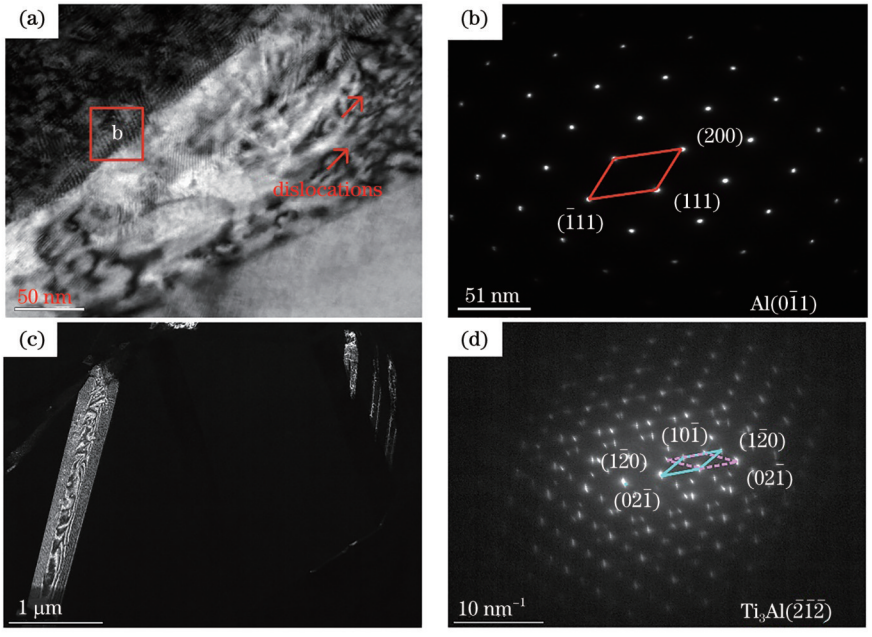

图 7　界面的 TEM 图像。(a)位错的 HAADF-STEM 图像;(b)位错区域的 SAED 模式;(c)孪晶 HAADF-STEM 图像;(d)孪晶的 SAED 模式

Fig. 7　TEM images of the interface. (a) HAADF-STEM image of dislocations; (b) SAED mode in dislocation region; (c) HAADF-STEM image of twinning; (d) twinning SAED mode

(270 MPa)的 1.4~4 倍。断裂前弹性变形量,复合结构应变为 3.3%~7.2%,是铝基体(2.1%)的 0.6~2.4 倍。

3) 铝-钛复合结构增强增韧的主要原因,一方面通过控制反应温度,界面内形成软相、硬相空间互穿相结构,在应力作用下软/硬区诱发 HDI 强化机制,且界面内为具有一定变形能力的 Ti_3Al 孪晶,进一步形成强韧性匹配很好的微/宏观界面。另一方面界面内较高模量的析出相周围形成了几何必要位错,有利于软/硬相之间协调变形。

4) 建立结构-性能的双向预测模型,值得一提的是这种加工方法可以扩展到成分具有不同熔点的任何金属系统中,为更精确、高效地设计和构建多金属体系提供理论依据。

参　考　文　献

[1]　Wang Y, Yang B W, Gao M Q, et al. Deformation behavior and

dynamic recrystallization during hot compression in homogenized Al-6Mg-0.8Mn alloys[J]. Materials Science and Engineering: A, 2022, 840: 142953.

[2] Guo C, Zhang H T, Li J H. Influence of Zn and/or Ag additions on microstructure and properties of Al-Mg based alloys[J]. Journal of Alloys and Compounds, 2022, 904: 163998.

[3] Zhu Z G, Hu Z H, Seet H L, et al. Recent progress on the additive manufacturing of aluminum alloys and aluminum matrix composites: Microstructure, properties, and applications[J]. International Journal of Machine Tools and Manufacture, 2023, 190: 104047.

[4] 武高辉, 匡泽洋. 装备升级换代背景下金属基复合材料的发展机遇和挑战[J]. 中国工程科学, 2020, 22(2): 79-90.
Wu G H, Kuang Z Y. Opportunities and challenges for metal matrix composites in the context of equipment upgrading[J]. Strategic Study of CAE, 2020, 22(2): 79-90.

[5] 石川, 雷剑波, 周圣丰, 等. 连续纤维增强金属基复合材料研究进展及其激光熔覆[J]. 激光与光电子学进展, 2017, 54(6): 060003.
Shi C, Lei J B, Zhou S F, et al. Research progress on continuous fiber-reinforced metal matrix composites and their laser cladding[J]. Laser & Optoelectronics Progress, 2017, 54(6): 060003.

[6] 陈琨, 马佳威, 齐硕, 等. 激光选区熔化成形 Al-Mg-Sc-Zr 合金的微观组织及力学性能[J]. 激光与光电子学进展, 2022, 59(21): 2116001.
Chen K, Ma J W, Qi S, et al. Microstructures and mechanical properties of Al-Mg-Sc-Zr alloy formed by selective laser melting [J]. Laser & Optoelectronics Progress, 2022, 59(21): 2116001.

[7] 邹田春, 祝贺, 陈敏英, 等. 激光选区熔化碳化硅增强铝基复合材料的微观组织及拉伸性能研究[J]. 中国激光, 2021, 48(10): 1002123.
Zou T C, Zhu H, Chen M Y, et al. Microstructure and tensile properties of SiC reinforced aluminum matrix composite prepared by selective laser melting[J]. Chinese Journal of Lasers, 2021, 48 (10): 1002123.

[8] 顾冬冬, 张红梅, 陈洪宇, 等. 航空航天高性能金属材料构件激光增材制造[J]. 中国激光, 2020, 47(5): 0500002.
Gu D D, Zhang H M, Chen H Y, et al. Laser additive manufacturing of high-performance metallic aerospace components [J]. Chinese Journal of Lasers, 2020, 47(5): 0500002.

[9] 梁家誉, 张文扬, 刘伟, 等. 热交换器点阵结构优化及其激光选区熔化成形[J]. 激光与光电子学进展, 2022, 59(19): 1914006.
Liang J Y, Zhang W Y, Liu W, et al. Optimization and laser selective melting for lattice structure of heat exchanger[J]. Laser & Optoelectronics Progress, 2022, 59(19): 1914006.

[10] 房立家, 孙兵兵, 张强, 等. 激光选区熔化成形零件结构设计与分析[J]. 激光与光电子学进展, 2023, 60(5): 0514010.
Fang L J, Sun B B, Zhang Q, et al. Structural design and analysis of selective laser melting forming parts[J]. Laser & Optoelectronics Progress, 2023, 60(5): 0514010.

[11] Yan X X, Bethers B, Chen H X, et al. Recent advancements in biomimetic 3D printing materials with enhanced mechanical properties[J]. Frontiers in Materials, 2021, 8: 139.

[12] Sun J X, Yu S X, Wade-Zhu J, et al. 3D printing of ceramic composite with biomimetic toughening design[J]. Additive Manufacturing, 2022, 58: 103027.

[13] Liu X C, Liu Z, Liu Y J, et al. Achieving high strength and toughness by engineering 3D artificial nacre-like structures inTi_6Al_4V-Ti metallic composite[J]. Composites Part B: Engineering, 2022, 230: 109552.

[14] Zhang Y, Tan G Q, Zhang M Y, et al. Bioinspired tungsten-copper composites with bouligand-type architectures mimicking fish scales[J]. Journal of Materials Science & Technology, 2022, 96: 21-30.

[15] Zhang M Y, Zhao N, Yu Q, et al. On the damage tolerance of 3-D printed Mg-Ti interpenetrating-phase composites with bioinspired architectures[J]. Nature Communications, 2022, 13: 3247.

[16] Chen C J, Li Z H, Mi R Y, et al. Rapid processing of whole bamboo with exposed, aligned nanofibrils toward a high-performance structural material[J]. ACS Nano, 2020, 14(5): 5194-5202.

[17] Li S H, Zeng Q Y, Xiao Y L, et al. Biomimicry of bamboo bast fiber with engineering composite materials[J]. Materials Science and Engineering: C, 1995, 3(2): 125-130.

[18] Lin C F, Wu W W, Han Y Q, et al. Orderly nucleation and competitive growth behaviors of Ti-Al intermetallic compounds in Ti/$TiAl_3$ diffusion couple under high temperature[J]. Journal of Alloys and Compounds, 2023, 939: 168815.

[19] Zhang H M, Zhang N N, Jia Q Q, et al. Calculation and experimentation on the formation sequence of compounds at Al/Ti interface in pure Al antioxidant coatings[J]. Materials Today Communications, 2020, 25: 101192.

[20] Yang W Y, Weatherly G C. A study of combustion synthesis of Ti-Al intermetallic compounds[J]. Journal of Materials Science, 1996, 31(14): 3707-3713.

[21] Sujata M, Bhargava S, Sangal S. On the formation of $TiAl_3$ during reaction between solid Ti and liquid Al[J]. Journal of Materials Science Letters, 1997, 16(14): 1175-1178.

[22] Li L, Xiao L R, Zhang D K, et al. Ductilization of a diffusion-bonded heterostructured AZ31/GW103K/AZ31 alloy by interfacial reinforcement[J]. Materials Science and Engineering: A, 2022, 852: 143691.

[23] Shao C W, Zhao S, Wang X G, et al. Architecture of high-strength aluminum-matrix composites processed by a novel microcasting technique[J]. NPG Asia Materials, 2019, 11: 69.

[24] Pawlowski A E, Cordero Z C, French M R, et al. Damage-tolerant metallic composites via melt infiltration of additively manufactured preforms[J]. Materials & Design, 2017, 127: 346-351.

[25] Tsopanos S, Mines R A W, McKown S, et al. The influence of processing parameters on the mechanical properties of selectively laser melted stainless steel microlattice structures[J]. Journal of Manufacturing Science and Engineering, 2010, 132(4): 041011.

[26] Smith M, Guan Z, Cantwell W J. Finite element modelling of the compressive response of lattice structures manufactured using the selective laser melting technique[J]. International Journal of Mechanical Sciences, 2013, 67: 28-41.

[27] Huang H F, Jiang F, Zhou J, et al. Effects of Al_3(Sc, Zr) and shear band formation on the tensile properties and fracture behavior of Al-Mg-Sc-Zr alloy[J]. Journal of Materials Engineering and Performance, 2015, 24(11): 4244-4252.

[28] Li W C, Cai H W, Kang Y, et al. High permeability and low loss bioinspired soft magnetic composites with nacre-like structure for high frequency applications[J]. Acta Materialia, 2019, 167: 267-274.

[29] Caminero M A, García-Moreno I, Rodríguez G P, et al. Internal damage evaluation of composite structures using phased array ultrasonic technique: impact damage assessment in CFRP and 3D printed reinforced composites[J]. Composites Part B: Engineering, 2019, 165: 131-142.

[30] Azarov A V, Antonov F K, Golubev M V, et al. Composite 3D printing for the small size unmanned aerial vehicle structure[J]. Composites Part B: Engineering, 2019, 169: 157-163.

[31] Xu Z H, Li X D. Deformation strengthening of biopolymer in nacre [J]. Advanced Functional Materials, 2011, 21(20): 3883-3888.

[32] Liu J L, Huang Z W, Pan Z L, et al. Atomistic origin of deformation twinning in biomineral aragonite[J]. Physical Review Letters, 2017, 118(10): 105501.

[33] Song N N, Zhang Y Y, Gao Z, et al. Bioinspired, multiscale reinforced composites with exceptionally high strength and toughness[J]. Nano Letters, 2018, 18(9): 5812-5820.

Strength-Toughness Modulation and Interfacial Microstructure of Bionic Bamboo Fiber-like Aluminum-Based Composite Structures (Invited)

Yang Guang[1*], Ma Yixin[1], Zhao Shuo[2**], Qin Lanyun[1], Wang Xiangming[3]

[1]*College of Mechanical and Electrical Engineering, Shenyang Aerospace University, Liaoning* 110136, *Shenyang, China*;

[2]*Key Laboratory of Fundamental Science for National Defense of Aeronautical Digital Manufacturing Process, Shenyang Aerospace University, Liaoning* 110136, *Shenyang, China*;

[3]*Shenyang Aircraft Design Institute, Aviation Industry Group Corporation, Liaoning* 110035, *Shenyang, China*

Abstract

Objective Aluminum matrix composites (AMCs) are widely used in the aerospace industry, transportation, electronics, and other fields because of their high specific strength, low cost, good corrosion resistance, and easy recyclability, which puts higher demands on their comprehensive performance to meet the damage tolerance design criteria. However, AMCs prepared by traditional methods are costly and complex, and the formed materials are prone to the phenomenon of mutual exclusion of strength and fracture toughness. To further improve the strength and toughness of AMCs and overcome the inverse relationship between them, in addition to the selection of the reinforcement material for the matrix, the preparation method and design of the spatial structure also play a crucial role in the construction of high-strength and high-toughness AMCs. The additive manufacturing method differs from the traditional preparation method in that it stacks layers of material onto a substrate and can obtain a free form by precisely regulating the phase evolution as well as the distribution of components and structures. Thus, as it can customize the structure and synthesize a variety of materials, this process is more suitable for developing heterogeneous structures. At the same time, bionic structures provide a new way of thinking for realizing high-performance materials by mimicking the regulation of existing microstructures in nature.

Methods By adding titanium alloy skeleton structures with different volume fractions and sizes to the aluminum matrix, strength- and toughness-adjustable bamboo fiber-like Al-Ti composite structures were prepared. The micro/macro interfacial organization of the composite structure was observed, the chemical composition and elemental distribution of each phase were analyzed, the coordinated deformation ability of the composite structure under compressive stress was studied, and the deformation and interfacial toughening mechanisms of the composite structure were elucidated.

Results and Discussions It is found that a diffusion reaction occurs in the interface of the titanium-alloy reinforcement skeleton and aluminum alloy matrix, forming a dense metallurgical bond, and the precipitated phases at the interface are Ti-Al intermetallic compounds (Fig. 3). Compared with traditional aluminum-matrix composite materials, this composite structure has a compressive strength as high as 380–1085 MPa and forms an integrated micro/macro "high strength-high toughness" fiber-like composite structure (Fig. 4). The study of the micro-deformation mechanism reveals that the precipitation of high-strength compounds effectively prevents cracks from sprouting and expanding in the heterogeneous interface (Fig. 5). Meanwhile, high-resolution observation shows that the Ti_3Al phase precipitated at the interface forms effective deformation twins inside the grains after deformation (Fig. 7) and improves the coordinated deformation ability between the high- and low-modulus phases precipitated at the interface. This is the main mechanism for the enhancement and toughening of the composite structure.

Conclusions By adjusting the vacuum melting temperature, an aluminum/titanium composite structure can be obtained with a dense combination of the interface. The thickness of the reaction-generated interface is approximately 600 μm, and the phase precipitated within the interface is a Ti-Al intermetallic compound with high hardness. The aluminum/titanium composite structure has good strength and toughness, and by adjusting the volume fraction of the titanium alloy skeleton, the macro-strength/toughness of the composite structure can be adapted. The achieved compressive strength varies in the range of 380–1085 MPa, which is 1.4–4 times that of the aluminum matrix (270 MPa). Regarding the pre-fracture elastic deformation, the strain of the composite structure is 3.3%–7.2%, which is 0.6–2.4 times that of the aluminum matrix (2.1%), and a bidirectional prediction model of structure-property is established. The main reasons for the enhanced toughening of the Al-Ti composite structure are as follows: First, by controlling the reaction temperature, a soft phase and hard phase spatially interpenetrating phase structure is formed in the interface, and this soft/hard zone induces the hetero-deformation induced (HDI) strengthening mechanism under the action of the stress. The Ti_3Al twins in the interface have certain deformation ability, which further forms a micro/macroscopic interface with a very good match of strength and toughness. Second, geometrically necessary dislocations are formed around the phases with higher modulus precipitated in the interface, which is favorable for the coordinated deformation between the soft and hard phases. It is worth mentioning that the processing method presented in this study can be extended to any metal system with compositions having different melting points, which can provide a theoretical basis for more accurate and efficient design and construction of multimetallic systems.

Key words laser technique; additive manufacturing; biomimetic structures; Al-Ti composite structural materials; micro/macro strength toughness modulation